Nuclear Science and Techniques (2024) 35:27
https://doi.org/10.1007/s41365-024-01371-y

α Decay in extreme laser fields within a deformed Gamow-like model

Qiong Xiao[1] · Jun-Hao Cheng[1] · Yang-Yang Xu[1] · You-Tian Zou[1] · Jun-Gang Deng[2] · Tong-Pu Yu[1]

Received: 14 July 2023 / Revised: 1 September 2023 / Accepted: 13 September 2023 / Published online: 29 February 2024

Abstract
In this study, the effect of extreme laser fields on the α decay process of ground-state even–even nuclei was investigated. Using the deformed Gamow-like model, we found that state-of-the-art lasers can cause a slight change in the α decay penetration probability of most nuclei. In addition, we studied the correlation between the rate of change of the α decay penetration probability and angle between the directions of the laser electric field and α particle emission for different nuclei. Based on this correlation, the average effect of extreme laser fields on the half-life of many nuclei with arbitrary α particle emission angles was calculated. The calculations show that the laser suppression and promotion effects on the α decay penetration probability of the nuclei population with completely random α particle-emission directions are not completely canceled. The remainder led to a change in the average penetration probability of the nuclei. Furthermore, the possibility of achieving a higher average rate of change by altering the spatial shape of the laser is explored. We conclude that circularly polarized lasers may be helpful in future experiments to achieve a more significant average rate of change of the α decay half-life of the nuclei population.

Keywords α Decay · Deformed Gamow-like model · Half-lives · Extreme laser field · Penetration probability

1 Introduction

α decay is highly significant in nuclear physics because of the information it can provide regarding the nuclear structure and stability [1–4]. This process involves the emission of an α particle (helium nucleus) by an unstable nucleus. Early interpretations of this process were provided by Gamow, Condon, and Gurney [5], who viewed it as a quantum tunneling effect. This is one of the earliest applications of quantum mechanics in nuclear physics [5, 6]. Recently, significant advancements have been made in both the theory and experimentation of α decay. Theoretically, α-decay shares a similar theory of barrier penetration with spontaneous fission, proton radioactivity, and heavy ion emission [7–10], which makes α-decay a critical tool for studying nuclear structures, e.g., from the barrier tunneling theory to the investigation of superheavy nuclei (SHN) [11–16], from the discovery of the nucleus by α scattering to the Geiger-Nuttall law [17, 18]. Experimentally, α-decay spectroscopy of heavy, superheavy, and neutron-deficient nuclei has become an important basis for the synthesis and identification of new nuclides formed in nuclear reactions [19–21]. Moreover, in astrophysics, studying α decay processes is crucial for understanding popular topics such as the chronology of the solar system [22] and stellar nucleosynthesis [23].

Another important assumption in the study of α decay is that emitted α particles are formed on the surface of the nucleus and eventually pass through the potential barrier through constant collisions with the potential barrier [24, 25]. The formation, collision, and penetration processes of α decay involve the complicated structure of many-body quantum systems. To better explain the α decay process, many models and formulas have been developed, such as

This work was supported by the National Nature Science Foundation of China (Nos. 12375244, 12135009), the Science and Technology Innovation Program of Hunan Province (No. 2020RC4020), and the Hunan Provincial Innovation Foundation for Postgraduate (No. CX20210007), Natural Science Research Project of Yichang City (No. A23-2-028).

✉ Jun-Hao Cheng
cjh452002@163.com

✉ Tong-Pu Yu
tongpu@nudt.edu.cn

[1] Department of Physics, National University of Defense Technology, Changsha 410073, China

[2] College of Science, China Three Gorges University, Yichang 443002, China

the generalized liquid drop model [24, 26–28], Gamow-like model [29–31], cluster model [32–34], the two-potential approach [35–37], the deformed version of the density-dependent cluster model (DDCM) with microscopic double-folding potentials [38–40], and empirical formulas [41–46], which reproduce the α decay half-life experimental data to some extent. However, because of the strong nucleon–nucleon interactions in the dense nuclear structure, previous studies of α decay have mainly observed and analyzed the behavior of the nucleus. Directly interfering with the natural decay of nuclei using conventional methods is challenging. Consequently, more effective tools are required to modulate the α decay of nuclei to obtain more information on the nuclear structure and a more comprehensive range of nuclei applications.

Since the invention of the chirped-pulse amplification (CPA) technology by Gerard Mourou and Donna Strickland [47], rapidly evolving laser technology has demonstrated its irreplaceable role in many fields such as nuclear physics, inertial confinement fusion, fusion ignition, medicine, and electron-positron pair production [48–53]. To date, significant progress has been made in the development of ultrashort, ultraintense laser pulses with pulse widths of less than 100 fs and intensities of up to 10^{23} W/cm^2 in a laboratory [54]. Moreover, the extreme light infrastructure (ELI) being constructed in Europe is expected to increase the laser intensity by one to two orders of magnitude [55, 56], providing a new platform for studying the interaction between lasers and matter in extreme laser field environments and enhancing laser-driven nuclear physics research.

In atomic-molecular physics, the interaction of lasers with matter is a well-established subject. The nonlinear reactions of molecules or atoms caused by laser fields constitute the research discipline of nonlinear optics [57]. However, in the microscopic field of nuclear physics, the direct reaction between the laser and nuclei has rarely been studied because the typical nuclear energy level is on the order of Mega-electron volts, and the energy of laser photons is much smaller than this value [58]. This gap has narrowed with the rapid developments of the laser technology. When the laser intensity reaches 10^{24} W/cm^2, the corresponding electric field strength is approximately equal to the Coulomb field strength of the nucleus near 100 fm. This implies that a direct interaction of the laser with the nucleus is possible [59–62]. Recently, extensive research has been conducted to study the direct effects of lasers on nuclei, e.g., nuclear excitation [63], refractive scattering of loosely bound nuclei [64], α decay [65–71], proton radioactivity [55, 72], nuclear fusion [73], nuclear fission [58], and modification of heavy-ion elastic-scattering differential cross sections [74]. This implies that an extreme laser-field environment offers a new tool for studying α decay. The most intriguing question is whether intense lasers can accelerate α decay, which, if feasible, would open up new possibilities for nuclear waste disposal. Another ongoing study of ours [71] explores the key factors of laser effects on the rate of change of the penetration probability of α decay of individual nuclei, that is, the properties of the nucleus and laser. However, in real applications where nuclei often appear as a population, the effect of lasers on a randomly emitted population of nuclei must be studied.

For a direct laser-nucleus interaction, an electric dipole term is introduced in the nuclear Hamiltonian, which is closely related to the angle ψ between the direction of the laser electric field and that of the α particle emission. Considering the nuclear deformation to study the laser effect on α decay is essential. In addition, the introduction of a new interaction term may be affected by the adjustable parameters. Therefore, more accurate results may be obtained using a model with minimal adjustable parameters to calculate the laser effect on α decay. In this study, we investigate the effect of an extreme laser field on the α decay of ground-state even–even nuclei based on the deformed Gamow-like model, which has only one adjustable parameter, radius constant r_0. Moreover, we study the relationship between ψ and the rate of change of the α decay half-life for different nuclei. Furthermore, the average effect of the extreme laser on the nuclei population's α decay penetration probability with arbitrary α particle-emission angles is calculated, and the possibility of obtaining a more effective average rate of change by changing the spatial shape of the laser is discussed.

The remainder of this paper is organized as follows: Section 2 introduces the deformed Gamow-like model and direct laser-nucleus interactions in detail. Section 3 presents the results and discussions. Section 4 presents the summary.

2 Theoretical framework

2.1 The deformed Gamow-like model

In the deformed Gamow-like model, the total penetration probability P is obtained by averaging $P(\theta)$ in all directions [38]

$$P = \frac{1}{2}\int_0^{\pi} P(\theta)\,\sin\theta \mathrm{d}\theta, \tag{1}$$

where θ denotes the orientation angle of the symmetry axis of the daughter nucleus with respect to the emitted α particles. The calculation of $P(\theta)$ in each direction is similar to that of the Gamow-like model [29, 30]; however, the Coulomb potential used for the calculations is more complex. $P(\theta)$ can be expressed as follows:

$$P(\theta) = \exp\left[-\frac{2}{\hbar}\int_{R_{\rm in}(\theta)}^{R_{\rm out}(\theta)}\sqrt{2\mu(V(r,\theta)-E_\alpha)}\,{\rm d}r\right], \tag{2}$$

where $\hbar$ denotes the reduced Planck constant, r is the separation between the mass center of the daughter nucleus and that of the emitted α particle, and the lower limit of integration $R_{\rm in}(\theta)$ is the radius of the square well, and can be expressed as

$$R_{\rm in}(\theta) = r_0 A_d^{\frac{1}{3}}(1+\beta_2 Y_{20}(\theta)+\beta_4 Y_{40}(\theta)+\beta_6 Y_{60}(\theta)) + r_0 A_\alpha^{\frac{1}{3}}, \tag{3}$$

The adjustable parameter radius constant $r_0 = 1.17$ fm was obtained from [75]. $A_{\rm d}$ and A_α represent the mass numbers of daughter nucleus and α particle, respectively. β_2, β_4, and β_6 are the calculated quadrupole, hexadecapole, and hexacontatetrapole deformation of the nuclei, respectively. The upper limit of the integration $R_{\rm out}(\theta)$ is the outer turning point, which can be obtained by

$$V(R_{\rm out}) = E_\alpha, \tag{4}$$

where $E_\alpha = Q_\alpha\frac{A-A_\alpha}{A}$ represents the kinetic energy of the emitted α particles. Q_α and A are the decay energy and mass of the parent nucleus, respectively.

The total potential between the emitted α particle and daughter nucleus $V(r,\theta)$ can be expressed as

$$V(r,\theta) = \begin{cases} -V_0, & 0 \le r \le R_{\rm in}(\theta), \\ V_{\rm C}(r,\theta)+V_l(r), & r > R_{\rm in}(\theta), \end{cases} \tag{5}$$

where V_0 is the potential well depth and $V_l(r)$ is the centrifugal potential, which can be expressed as

$$V_l(r) = \frac{l(l+1)\hbar^2}{2\mu r^2}, \tag{6}$$

where $\mu = \frac{m_{\rm d}m_\alpha}{(m_{\rm d}+m_\alpha)}$ is the reduced mass and $m_{\rm d}$ and m_α represent the masses of the daughter nucleus and emitted α particle, respectively. l is the orbital angular momentum of the emitted α-particle. In this study, we only focused on the α decay of the ground-state even–even nuclei; thus, $l = 0$ was considered in the calculations. The Coulomb potential $V_{\rm C}(r,\theta)$ was calculated using the double-folding model [38–40], which is expressed as:

$$V_{\rm C}(r,\theta) = \int\int \frac{\rho_1(\vec{r}_1)\rho_2(\vec{r}_2)}{|\,\mathbf{r}-\vec{r}_2+\vec{r}_1\,|}{\rm d}\vec{r}_1{\rm d}\vec{r}_2, \tag{7}$$

where $\vec{r}_1$ and ρ_1 represent the radius vector and the density distribution of the daughter nucleus, respectively. $\vec{r}_2$ and ρ_2 represent the radius vector and density distribution of the emitted α particle, respectively. Simplified appropriately by the Fourier transform [76–78], the Coulomb potential can be approximated as

$$V_{\rm C}(r,\theta) = V_{\rm C}^{(0)}(r,\theta)+V_{\rm C}^{(1)}(r,\theta)+V_{\rm C}^{(2)}(r,\theta), \tag{8}$$

where $V_{\rm C}^{(0)}(r,\theta)$, $V_{\rm C}^{(1)}(r,\theta)$ and $V_{\rm C}^{(2)}(r,\theta)$ represent the bare Coulomb interactions, linear Coulomb coupling, and second-order Coulomb coupling, respectively [76].

In the deformed Gamow-like model, the even–even nuclei α decay half-lives are expressed as

$$T_{\frac{1}{2}} = \frac{\ln 2}{\lambda}, \tag{9}$$

where decay constant λ depends on the α-particle-formation probability S_α, collision frequency ν, and penetration probability P [46].

$$\lambda = S_\alpha \nu P, \tag{10}$$

$S_\alpha = 0.5$ is obtained from [75]. ν can be calculated using the oscillation frequency ω_α [79]

$$\nu = \omega_\alpha/2\pi = \frac{(2n_{\rm r}+l+\frac{3}{2})\hbar}{2\pi\mu {R_{\rm n}}^2} = \frac{(G+\frac{3}{2})\hbar}{1.2\pi\mu {R_0}^2}, \tag{11}$$

where $R_{\rm n} = \sqrt{3/5}R_0$ denotes the root-mean-square radius of the nucleus, with the radius of the parent nucleus $R_0 = 1.28A^{1/3} - 0.76 + 0.8A^{-1/3}$. Moreover, $G = 2n_{\rm r} + l$ is the main quantum number [80] and $n_{\rm r}$ is the radial quantum number of the emitted particle.

2.2 Laser–nucleus interaction

In an extreme laser field environment, the total potential $V(r,\theta,t,\psi)$ between the emitted α particle and daughter nucleus can be rewritten as

$$V(r,\theta) = \begin{cases} -V_0, & 0 \le r \le R_{\rm in}(\theta), \\ V_{\rm C}(r,\theta)+V_l(r)+V_i(r,t,\psi), & r > R_{\rm in}(\theta), \end{cases} \tag{12}$$

where the electric dipole term $V_i(r,t,\psi)$ is expressed as [66]

$$V_i(r,t,\psi) = -Z_{\rm eff}\,\vec{r}\cdot\vec{E}(t) = -Z_{\rm eff} rE(t)\cos\psi, \tag{13}$$

where $Z_{\rm eff}$ is the effective charge, which represents the tendency of the laser electric field to separate the emitted α -particle. This can be expressed as

$$Z_{\rm eff} = \frac{Z_\alpha A_{\rm d} - Z_{\rm d}A_\alpha}{A_{\rm d}+A_\alpha}, \tag{14}$$

where $Z_{\rm d}$ and Z_α are the proton numbers of the daughter nucleus and emitted α particle, respectively. If the daughter nucleus and emitted α particle have the same charge-to-mass ratio, they move cooperatively in the laser field, and the laser electric field does not separate the two particles.

In this study, the laser electric field was obtained using

$$E(t) = E_0 f(t)\sin(\omega t), \tag{15}$$

where ω and E_0 represent the angular frequency and peak of the laser electric field, respectively. The peak of the laser electric field intensity E_0 is related to the peak of the laser intensity I_0, which is expressed as [55]

$$E_0[\mathrm{V\,cm^{-1}}] = \left(\frac{2I_0}{c\epsilon_0}\right)^{1/2} = 27.44(I_0[\mathrm{W\,cm^{-2}}])^{1/2}, \tag{16}$$

where c and ϵ_0 represent the speed of light in vacuum and the permittivity of free space, respectively. A high-energy laser pulse has a Gaussian shape [54, 81], which can be expressed as

$$f(t) = \exp\left(-\frac{t^2}{\tau^2}\right), \tag{17}$$

where the pulse width of the envelope is $\tau = xT_0$ and T_0 is the pulse period.

In an extreme laser field environment, the kinetic energy of the emitted α particle can be altered by the laser electric field. The change in kinetic energy is related to the laser electric field, and E_α can be rewritten as

$$E_\alpha^i = Q_\alpha \frac{A - A_\alpha}{A} + eE(t)R_{\mathrm{in}}(\theta)\cos\psi. \tag{18}$$

Figure 1 is the schematic diagram depicting the total potential V with and without considering the laser electric field. The blue and red curves represent the total potential $V(r,\theta)$ without considering the laser electric field and the total potential $V(r,\theta,t,\psi)$ with the laser electric field, respectively. R_{out} and E_α correspond to the outer turning point and α decay energy, respectively, without considering the laser. R_{out}^i and E_α^i are the outer turning point and α-decay energy, respectively, when the laser is considered. Figure 1 shows that the laser electric field directly affects the emitted α kinetic energy and total potential, thus changing the position of the classical turning point. The equation for calculating the penetration probability P is an exponential function sensitive to the kinetic energy of the emitted particle and position of the outer turning point. Therefore, the rate of change of the penetration probability P depends on the change in the kinetic energy of the emitted particle and change in the position of the outer turning point. This figure shows that the magnitudes of the two changes are related to the α decay process and laser intensity; therefore, the change in the penetration probability depends on the energy of the α particle and intensity of the laser field.

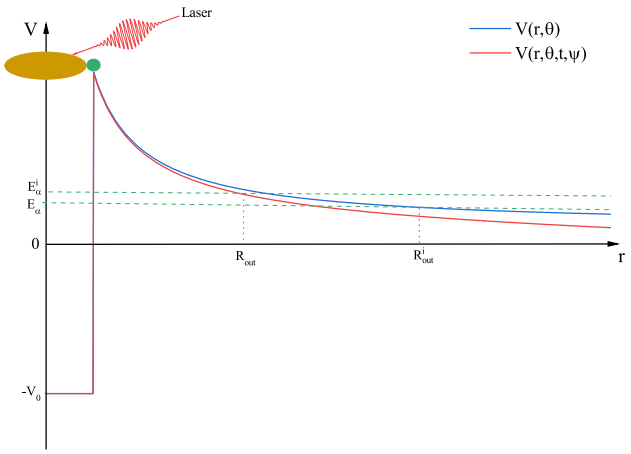

Fig. 1 (Color online) Schematic diagram of the total potential V with and without considering the laser electric field

3 Results and discussion

In this study, we first discuss the effect of the magnetic field of the laser on α decay. The kinetic energy of a typical emitted α particle is approximately a few Mega-electron volts, which means that the speed of the emitted α particle is much lower than the speed of light in vacuum. Compared to the electric-field part of the laser, the magnetic field of the laser has a minor effect and can be disregarded. During α decay, the emitted α particle oscillates within the parent nucleus at a high frequency and ultimately escapes the quantum-tunneling effect. The size of the parent nucleus is on the order of 1 fm, and the oscillation frequency of the emitted α particles is estimated to be approximately 10^{22} Hz. Considering that the length of the tunneling process is less than 100 fm, the time required to emit α particles is less than 10^{-20} s. This timescale is much smaller than the currently achievable highest peak-intensity laser-pulse period [58]. Therefore, we treat the laser field as quasi-static, that is, the laser field remains constant throughout α decay.

The rate of change of the α decay half-life δT is used to define the effect of the laser electric field on the α decay half-life and is written as

$$\delta T = \frac{T(E) - T(E=0)}{T(E=0)}, \tag{19}$$

where $T(E)$ and $T(E=0)$ represent the theoretical half-lives with and without the laser electric field, respectively. Similarly, the rate of change of the penetration probability δP is written as

$$\delta P = \frac{P(E) - P(E=0)}{P(E=0)}, \tag{20}$$

where $P(E)$ and $P(E=0)$ represent the theoretical penetration probabilities with and without the laser electric field,

respectively. Because the collision of the α-particle with the potential barrier occurs inside the nucleus, collision frequency ν is insensitive to the external laser field. Therefore, we assume that the laser field changes the half-life of the α decay mainly by affecting the α decay penetration probability. δT can be represented by $P(E)$ and $P(E=0)$

$$\delta T = \frac{P(E=0) - P(E)}{P(E)}. \tag{21}$$

We studied δP and δT of the α decay of the ground-state even–even nuclei with laser intensities of $I = 10^{23}$ W/cm^2 and $I = 10^{24}$ W/cm^2. The detailed results are presented in Table 1. The α decay energy Q_α used in the calculations was obtained from AME2020 [82, 83]. The quadrupole deformation β_2, hexadecapole deformation β_4 and hexacontatetrapole deformation β_6 were obtained from FRDM2012 [84]. The angle ψ between the direction of the laser electric field and that of the α-particle emission was set to zero. In Table 1, the first three columns represent the parent nuclei, α-decay energy Q_α, and theoretical penetration probability value P without the laser field. The next three columns represent the theoretical penetration probability value P^{23} for laser intensities $I = 10^{23}$ W/cm^2 and the corresponding δP^{23} and δT^{23}, respectively. The last three columns represent the theoretical penetration probability value P^{24} for a laser intensity of $I = 10^{24}$ W/cm^2 and the corresponding δP^{24} and δT^{24}, respectively.

Table 1 shows that laser electric fields with intensities of $I = 10^{23}$ W/cm^2 and $I = 10^{24}$ W/cm^2 can cause a slight change in the α decay penetration probability of most parent nuclei. However, ^{108}Xe is not affected by the laser electric field because it has a mass number twice the proton number, resulting in $Z_{\text{eff}} = 0$. This makes ^{108}Xe an exception, with δP and δT values of zero for any laser field intensity. Moreover, the parent nucleus that was the most sensitive to the laser electric field was ^{144}Nd, which had the lowest decay energy. For a fixed laser intensity, the smaller the decay energy, the larger the relative rate of change of the α -particle energy, according to Eq. (18). The schematics in Fig. 1, show that a smaller decay energy corresponds to a larger rate of change of the penetration probability P. This supports the findings of [72], which suggested that decay energy is inversely proportional to δP. Although ^{144}Nd already corresponds to δT in the order of thousands of parts in the case of $I = 10^{24}$ W/cm^2, the angle between the laser electric field direction and the α particle-emission direction was not always zero in the experiments. Therefore, it is more meaningful to study the effects of a laser on the emitted α particles in any direction.

In this study, we investigated the correlation between δP and ψ for ground-state even–even nuclei when $I = 10^{23}$ W/cm^2. The calculation results are shown in Fig. 2, where ψ ranges from zero to 2π, and each blue line represents the variation of a different parent nucleus δP with ψ. This figure shows that δP has a maximum value when $\psi = 0$, that is, the α particle-emission direction is the same as the laser electric field direction. In contrast, when the direction of the α particle emission is opposite to the direction of the laser electric field, that is, $\psi = \pi$, δP has a minimum value, and its absolute value is almost equal to the maximum value of δP. Moreover, the α particle-emission and laser electric field directions are perpendicular to each other in the case of $\psi = 1/2\pi$ or $\psi = 3/2\pi$ and the laser has almost no effect on the α decay penetration probability. Although δP varies for different nuclei at the same laser intensity, it exhibits a similar trend in the variation of δP with ψ, which is similar to that of cosψ with ψ, indicating a possible linear relationship between δP and cosψ.

Practical experiments involve studying the interactions between lasers and multiple nuclei (nuclei population). However, previous studies on laser–nucleus interactions have focused on individual nuclei and overlooked the effect of the laser on the nuclei population [71]. The effect of the laser on the penetration probability of α decay is closely related to the angle between the laser and α particle-emission direction, making the incident direction of the laser an interesting topic to explore. In this study, we investigated the average effect on the penetration probability δP_{avg} of the nuclei population with a laser intensity of $I = 10^{23}$ W/cm^2 in a specific direction. We assumed that the number of parent nuclei was sufficiently large and that the emission direction of the particles was entirely random. The calculation results are shown in Fig. 3, where the horizontal coordinate represents the mass number of the parent nuclei and the vertical coordinate represents the corresponding δP_{avg}.

Because the direction of the laser is fixed and the emission direction of the α particle is random, the effect of the laser on the α decay penetration probability of a nucleus in the nuclei population depends on ψ. When cos$\psi > 0$, the laser increases the α decay penetration probability; however, when cos$\psi < 0$, the laser decreases it. This implies that a fixed laser direction has both suppressive and facilitative effects on the α decay penetration probability of the parent nucleus in the nuclei population. If the relationship between δP and the laser electric field is linear, then the average value of the rate of change of the penetration probability in all directions is zero. However, Eq. (2) is an exponential function, and the absolute value of δP corresponding to the two cases (e.g., $\psi = 0$ and $\psi = \pi$) in which the α particle emission direction is at a completely opposite angle to the laser direction is different for the same nucleus. To further visualize this point, considering the nucleus ^{144}Nd, we calculated the absolute value of δP corresponding to the case of increasing or decreasing E_α using the same value, and the calculations were plotted in Fig. 4. In this figure, the

Table 1 Influence of a laser pulse with an intensity of 10^{23} W/cm^2 and 10^{24} W/cm^2 on the α decay of the ground-state even–even nuclei

Nucleus ^AZ	Q_p (MeV)	P	$I = 10^{23}$ W/cm^2			$I = 10^{24}$ W/cm^2		
			P^{23}	δP^{23}	δT^{23}	P^{24}	δP^{24}	δT^{24}
^{106}Te	4.29	7.542×10^{-19}	7.543×10^{-19}	1.501×10^{-4}	-1.501×10^{-4}	7.546×10^{-19}	4.774×10^{-4}	-4.772×10^{-4}
^{108}Te	3.42	1.401×10^{-23}	1.401×10^{-23}	2.354×10^{-4}	-2.353×10^{-4}	1.402×10^{-23}	7.446×10^{-4}	-7.441×10^{-4}
^{108}Xe	4.57	1.152×10^{-18}	1.152×10^{-18}	0	0	1.152×10^{-18}	0	0
^{110}Xe	3.872	5.981×10^{-22}	5.982×10^{-22}	1.915×10^{-4}	-1.914×10^{-4}	5.985×10^{-22}	6.077×10^{-4}	-6.073×10^{-4}
^{112}Xe	3.33	2.523×10^{-25}	2.523×10^{-25}	2.650×10^{-4}	-2.650×10^{-4}	2.525×10^{-25}	8.377×10^{-4}	-8.370×10^{-4}
^{114}Ba	3.592	9.200×10^{-25}	9.202×10^{-25}	2.298×10^{-4}	-2.297×10^{-4}	9.206×10^{-25}	7.274×10^{-4}	-7.268×10^{-4}
^{144}Nd	1.901	4.281×10^{-46}	4.287×10^{-46}	1.496×10^{-3}	-1.494×10^{-3}	4.301×10^{-46}	4.740×10^{-3}	-4.717×10^{-3}
^{146}Sm	2.529	2.925×10^{-38}	2.927×10^{-38}	8.304×10^{-4}	-8.297×10^{-4}	2.932×10^{-38}	2.629×10^{-3}	-2.622×10^{-3}
^{148}Sm	1.987	2.142×10^{-46}	2.145×10^{-46}	1.420×10^{-3}	-1.418×10^{-3}	2.151×10^{-46}	4.496×10^{-3}	-4.476×10^{-3}
^{148}Gd	3.271	5.715×10^{-32}	5.717×10^{-32}	4.977×10^{-4}	-4.974×10^{-4}	5.724×10^{-32}	1.577×10^{-3}	-1.574×10^{-3}
^{150}Gd	2.807	1.679×10^{-36}	1.680×10^{-36}	7.012×10^{-4}	-7.007×10^{-4}	1.683×10^{-36}	2.216×10^{-3}	-2.211×10^{-3}
^{152}Gd	2.204	3.504×10^{-44}	3.508×10^{-44}	1.224×10^{-3}	-1.222×10^{-3}	3.517×10^{-44}	3.874×10^{-3}	-3.859×10^{-3}
^{150}Dy	4.351	1.670×10^{-25}	1.670×10^{-25}	2.900×10^{-4}	-2.899×10^{-4}	1.671×10^{-25}	9.164×10^{-4}	-9.156×10^{-4}
^{152}Dy	3.727	1.462×10^{-29}	1.463×10^{-29}	4.008×10^{-4}	-4.006×10^{-4}	1.464×10^{-29}	1.273×10^{-3}	-1.271×10^{-3}
^{154}Dy	2.945	3.564×10^{-36}	3.566×10^{-36}	6.811×10^{-4}	-6.806×10^{-4}	3.571×10^{-36}	2.156×10^{-3}	-2.151×10^{-3}
^{152}Er	4.934	1.887×10^{-23}	1.887×10^{-23}	2.301×10^{-4}	-2.300×10^{-4}	1.888×10^{-23}	7.278×10^{-4}	-7.273×10^{-4}
^{154}Er	4.28	5.033×10^{-27}	5.035×10^{-27}	3.100×10^{-4}	-3.099×10^{-4}	5.038×10^{-27}	9.818×10^{-4}	-9.809×10^{-4}
^{156}Er	3.481	1.581×10^{-32}	1.582×10^{-32}	4.891×10^{-4}	-4.889×10^{-4}	1.584×10^{-32}	1.548×10^{-3}	-1.546×10^{-3}
^{154}Yb	5.474	6.059×10^{-22}	6.060×10^{-22}	1.910×10^{-4}	-1.909×10^{-4}	6.062×10^{-22}	6.032×10^{-4}	-6.029×10^{-4}
^{156}Yb	4.81	4.774×10^{-25}	4.776×10^{-25}	2.510×10^{-4}	-2.510×10^{-4}	4.778×10^{-25}	7.943×10^{-4}	-7.937×10^{-4}
^{156}Hf	6.026	1.282×10^{-20}	1.282×10^{-20}	1.608×10^{-4}	-1.608×10^{-4}	1.283×10^{-20}	5.088×10^{-4}	-5.086×10^{-4}
^{158}Hf	5.405	4.150×10^{-23}	4.151×10^{-23}	2.039×10^{-4}	-2.039×10^{-4}	4.152×10^{-23}	6.451×10^{-4}	-6.447×10^{-4}
^{160}Hf	4.902	1.980×10^{-25}	1.981×10^{-25}	2.559×10^{-4}	-2.558×10^{-4}	1.982×10^{-25}	8.102×10^{-4}	-8.095×10^{-4}
^{162}Hf	4.416	4.002×10^{-28}	4.003×10^{-28}	3.231×10^{-4}	-3.230×10^{-4}	4.006×10^{-28}	1.022×10^{-3}	-1.021×10^{-3}
^{174}Hf	2.494	4.670×10^{-46}	4.676×10^{-46}	1.223×10^{-3}	-1.222×10^{-3}	4.688×10^{-46}	3.872×10^{-3}	-3.857×10^{-3}
^{158}W	6.613	2.349×10^{-19}	2.349×10^{-19}	1.371×10^{-4}	-1.370×10^{-4}	2.350×10^{-19}	4.328×10^{-4}	-4.326×10^{-4}
^{160}W	6.066	2.848×10^{-21}	2.849×10^{-21}	1.657×10^{-4}	-1.657×10^{-4}	2.850×10^{-21}	5.237×10^{-4}	-5.234×10^{-4}
^{162}W	5.678	9.691×10^{-23}	9.693×10^{-23}	1.955×10^{-4}	-1.954×10^{-4}	9.697×10^{-23}	6.170×10^{-4}	-6.166×10^{-4}
^{164}W	5.278	1.750×10^{-24}	1.751×10^{-24}	2.312×10^{-4}	-2.312×10^{-4}	1.752×10^{-24}	7.319×10^{-4}	-7.314×10^{-4}
^{166}W	4.856	1.359×10^{-26}	1.359×10^{-26}	2.792×10^{-4}	-2.792×10^{-4}	1.360×10^{-26}	8.842×10^{-4}	-8.834×10^{-4}
^{168}W	4.501	1.423×10^{-28}	1.423×10^{-28}	3.339×10^{-4}	-3.338×10^{-4}	1.424×10^{-28}	1.059×10^{-3}	-1.057×10^{-3}
^{180}W	2.515	2.347×10^{-47}	2.350×10^{-47}	1.275×10^{-3}	-1.274×10^{-3}	2.356×10^{-47}	4.038×10^{-3}	-4.022×10^{-3}
^{162}Os	6.768	1.429×10^{-19}	1.429×10^{-19}	1.373×10^{-4}	-1.373×10^{-4}	1.430×10^{-19}	4.330×10^{-4}	-4.328×10^{-4}
^{164}Os	6.479	1.798×10^{-20}	1.798×10^{-20}	1.544×10^{-4}	-1.544×10^{-4}	1.798×10^{-20}	4.874×10^{-4}	-4.871×10^{-4}
^{166}Os	6.143	1.180×10^{-21}	1.180×10^{-21}	1.762×10^{-4}	-1.762×10^{-4}	1.181×10^{-21}	5.562×10^{-4}	-5.559×10^{-4}
^{168}Os	5.816	6.202×10^{-23}	6.203×10^{-23}	2.006×10^{-4}	-2.005×10^{-4}	6.206×10^{-23}	6.341×10^{-4}	-6.337×10^{-4}
^{170}Os	5.537	4.158×10^{-24}	4.159×10^{-24}	2.264×10^{-4}	-2.263×10^{-4}	4.161×10^{-24}	7.164×10^{-4}	-7.158×10^{-4}
^{172}Os	5.224	1.529×10^{-25}	1.529×10^{-25}	2.606×10^{-4}	-2.605×10^{-4}	1.530×10^{-25}	8.244×10^{-4}	-8.237×10^{-4}
^{174}Os	4.871	2.312×10^{-27}	2.313×10^{-27}	3.065×10^{-4}	-3.064×10^{-4}	2.314×10^{-27}	9.696×10^{-4}	-9.686×10^{-4}
^{186}Os	2.821	1.183×10^{-44}	1.184×10^{-44}	1.062×10^{-3}	-1.061×10^{-3}	1.187×10^{-44}	3.360×10^{-3}	-3.348×10^{-3}
^{166}Pt	7.292	1.319×10^{-18}	1.320×10^{-18}	1.254×10^{-4}	-1.254×10^{-4}	1.320×10^{-18}	3.940×10^{-4}	-3.939×10^{-4}
^{168}Pt	6.99	1.720×10^{-19}	1.720×10^{-19}	1.391×10^{-4}	-1.391×10^{-4}	1.720×10^{-19}	4.399×10^{-4}	-4.397×10^{-4}
^{170}Pt	6.707	2.211×10^{-20}	2.211×10^{-20}	1.550×10^{-4}	-1.550×10^{-4}	2.212×10^{-20}	4.894×10^{-4}	-4.892×10^{-4}
^{172}Pt	6.463	3.459×10^{-21}	3.459×10^{-21}	1.709×10^{-4}	-1.709×10^{-4}	3.461×10^{-21}	5.402×10^{-4}	-5.399×10^{-4}
^{174}Pt	6.183	3.330×10^{-22}	3.330×10^{-22}	1.908×10^{-4}	-1.908×10^{-4}	3.332×10^{-22}	6.036×10^{-4}	-6.032×10^{-4}
^{176}Pt	5.885	2.235×10^{-23}	2.236×10^{-23}	2.153×10^{-4}	-2.152×10^{-4}	2.237×10^{-23}	6.811×10^{-4}	-6.806×10^{-4}

Table 1 (continued)

Nucleus ^{A}Z	Q_p (MeV)	P	$I = 10^{23}$ W/cm^2			$I = 10^{24}$ W/cm^2		
			P^{23}	δP^{23}	δT^{23}	P^{24}	δP^{24}	δT^{24}
^{178}Pt	5.573	1.089×10^{-24}	1.090×10^{-24}	2.457×10^{-4}	-2.457×10^{-4}	1.090×10^{-24}	7.781×10^{-4}	-7.775×10^{-4}
^{180}Pt	5.276	4.093×10^{-26}	4.094×10^{-26}	2.793×10^{-4}	-2.793×10^{-4}	4.096×10^{-26}	8.835×10^{-4}	-8.827×10^{-4}
^{182}Pt	4.951	7.896×10^{-28}	7.898×10^{-28}	3.229×10^{-4}	-3.228×10^{-4}	7.904×10^{-28}	1.022×10^{-3}	-1.021×10^{-3}
^{184}Pt	4.599	6.658×10^{-30}	6.660×10^{-30}	3.816×10^{-4}	-3.815×10^{-4}	6.666×10^{-30}	1.207×10^{-3}	-1.205×10^{-3}
^{186}Pt	4.32	9.991×10^{-32}	9.995×10^{-32}	4.411×10^{-4}	-4.409×10^{-4}	1.001×10^{-31}	1.396×10^{-3}	-1.394×10^{-3}
^{188}Pt	4.007	5.250×10^{-34}	5.252×10^{-34}	5.245×10^{-4}	-5.242×10^{-4}	5.258×10^{-34}	1.659×10^{-3}	-1.656×10^{-3}
^{190}Pt	3.269	8.531×10^{-41}	8.538×10^{-41}	8.078×10^{-4}	-8.072×10^{-4}	8.553×10^{-41}	2.556×10^{-3}	-2.550×10^{-3}
^{170}Hg	7.77	6.641×10^{-18}	6.642×10^{-18}	1.154×10^{-4}	-1.154×10^{-4}	6.643×10^{-18}	3.636×10^{-4}	-3.635×10^{-4}
^{172}Hg	7.524	1.478×10^{-18}	1.478×10^{-18}	1.262×10^{-4}	-1.262×10^{-4}	1.479×10^{-18}	3.981×10^{-4}	-3.979×10^{-4}
^{174}Hg	7.233	2.085×10^{-19}	2.086×10^{-19}	1.391×10^{-4}	-1.390×10^{-4}	2.086×10^{-19}	4.393×10^{-4}	-4.391×10^{-4}
^{176}Hg	6.897	1.818×10^{-20}	1.818×10^{-20}	1.560×10^{-4}	-1.560×10^{-4}	1.819×10^{-20}	4.930×10^{-4}	-4.927×10^{-4}
^{178}Hg	6.577	1.561×10^{-21}	1.561×10^{-21}	1.755×10^{-4}	-1.755×10^{-4}	1.562×10^{-21}	5.547×10^{-4}	-5.544×10^{-4}
^{180}Hg	6.259	1.639×10^{-22}	1.639×10^{-22}	2.023×10^{-4}	-2.023×10^{-4}	1.640×10^{-22}	6.401×10^{-4}	-6.397×10^{-4}
^{182}Hg	5.996	1.487×10^{-23}	1.488×10^{-23}	2.245×10^{-4}	-2.245×10^{-4}	1.488×10^{-23}	7.103×10^{-4}	-7.098×10^{-4}
^{184}Hg	5.66	4.788×10^{-25}	4.789×10^{-25}	2.554×10^{-4}	-2.553×10^{-4}	4.792×10^{-25}	8.084×10^{-4}	-8.077×10^{-4}
^{186}Hg	5.204	2.070×10^{-27}	2.070×10^{-27}	3.029×10^{-4}	-3.028×10^{-4}	2.072×10^{-27}	9.591×10^{-4}	-9.582×10^{-4}
^{188}Hg	4.709	2.907×10^{-30}	2.908×10^{-30}	3.755×10^{-4}	-3.753×10^{-4}	2.910×10^{-30}	1.189×10^{-3}	-1.188×10^{-3}
^{178}Pb	7.789	1.847×10^{-18}	1.847×10^{-18}	1.252×10^{-4}	-1.251×10^{-4}	1.848×10^{-18}	3.946×10^{-4}	-3.945×10^{-4}
^{180}Pb	7.419	1.555×10^{-19}	1.555×10^{-19}	1.397×10^{-4}	-1.397×10^{-4}	1.556×10^{-19}	4.422×10^{-4}	-4.420×10^{-4}
^{182}Pb	7.066	1.203×10^{-20}	1.204×10^{-20}	1.569×10^{-4}	-1.569×10^{-4}	1.204×10^{-20}	4.963×10^{-4}	-4.961×10^{-4}
^{184}Pb	6.774	1.270×10^{-21}	1.271×10^{-21}	1.740×10^{-4}	-1.740×10^{-4}	1.271×10^{-21}	5.503×10^{-4}	-5.500×10^{-4}
^{186}Pb	6.471	1.022×10^{-22}	1.022×10^{-22}	1.943×10^{-4}	-1.943×10^{-4}	1.023×10^{-22}	6.145×10^{-4}	-6.141×10^{-4}
^{188}Pb	6.109	3.619×10^{-24}	3.620×10^{-24}	2.216×10^{-4}	-2.216×10^{-4}	3.622×10^{-24}	7.007×10^{-4}	-7.002×10^{-4}
^{190}Pb	5.698	5.321×10^{-26}	5.322×10^{-26}	2.588×10^{-4}	-2.587×10^{-4}	5.325×10^{-26}	8.179×10^{-4}	-8.172×10^{-4}
^{192}Pb	5.222	2.029×10^{-28}	2.029×10^{-28}	3.127×10^{-4}	-3.126×10^{-4}	2.031×10^{-28}	9.885×10^{-4}	-9.876×10^{-4}
^{194}Pb	4.738	2.716×10^{-31}	2.717×10^{-31}	3.853×10^{-4}	-3.851×10^{-4}	2.719×10^{-31}	1.219×10^{-3}	-1.217×10^{-3}
^{210}Pb	3.792	2.882×10^{-38}	2.884×10^{-38}	7.098×10^{-4}	-7.093×10^{-4}	2.889×10^{-38}	2.249×10^{-3}	-2.244×10^{-3}
^{186}Po	8.501	3.967×10^{-17}	3.968×10^{-17}	1.147×10^{-4}	-1.147×10^{-4}	3.969×10^{-17}	3.628×10^{-4}	-3.626×10^{-4}
^{188}Po	8.082	3.150×10^{-18}	3.150×10^{-18}	1.285×10^{-4}	-1.284×10^{-4}	3.151×10^{-18}	4.064×10^{-4}	-4.062×10^{-4}
^{190}Po	7.693	2.446×10^{-19}	2.446×10^{-19}	1.435×10^{-4}	-1.435×10^{-4}	2.447×10^{-19}	4.549×10^{-4}	-4.547×10^{-4}
^{192}Po	7.32	1.722×10^{-20}	1.722×10^{-20}	1.606×10^{-4}	-1.605×10^{-4}	1.722×10^{-20}	5.096×10^{-4}	-5.094×10^{-4}
^{194}Po	6.987	1.337×10^{-21}	1.337×10^{-21}	1.788×10^{-4}	-1.787×10^{-4}	1.338×10^{-21}	5.674×10^{-4}	-5.670×10^{-4}
^{196}Po	6.658	8.746×10^{-23}	8.748×10^{-23}	2.022×10^{-4}	-2.022×10^{-4}	8.752×10^{-23}	6.354×10^{-4}	-6.350×10^{-4}
^{198}Po	6.31	3.753×10^{-24}	3.754×10^{-24}	2.276×10^{-4}	-2.276×10^{-4}	3.755×10^{-24}	7.189×10^{-4}	-7.184×10^{-4}
^{200}Po	5.982	1.487×10^{-25}	1.487×10^{-25}	2.562×10^{-4}	-2.561×10^{-4}	1.488×10^{-25}	8.113×10^{-4}	-8.106×10^{-4}
^{202}Po	5.701	7.528×10^{-27}	7.530×10^{-27}	2.878×10^{-4}	-2.877×10^{-4}	7.535×10^{-27}	9.096×10^{-4}	-9.088×10^{-4}
^{204}Po	5.485	6.552×10^{-28}	6.554×10^{-28}	3.153×10^{-4}	-3.152×10^{-4}	6.558×10^{-28}	1.000×10^{-3}	-9.991×10^{-4}
^{206}Po	5.327	1.021×10^{-28}	1.022×10^{-28}	3.417×10^{-4}	-3.416×10^{-4}	1.022×10^{-28}	1.082×10^{-3}	-1.081×10^{-3}
^{208}Po	5.216	2.683×10^{-29}	2.684×10^{-29}	3.618×10^{-4}	-3.617×10^{-4}	2.686×10^{-29}	1.148×10^{-3}	-1.147×10^{-3}
^{210}Po	5.408	3.406×10^{-28}	3.407×10^{-28}	3.424×10^{-4}	-3.423×10^{-4}	3.410×10^{-28}	1.089×10^{-3}	-1.087×10^{-3}
^{212}Po	8.954	1.834×10^{-15}	1.834×10^{-15}	1.299×10^{-4}	-1.299×10^{-4}	1.834×10^{-15}	4.098×10^{-4}	-4.097×10^{-4}
^{214}Po	7.834	2.035×10^{-18}	2.036×10^{-18}	1.709×10^{-4}	-1.708×10^{-4}	2.036×10^{-18}	5.410×10^{-4}	-5.407×10^{-4}
^{216}Po	6.906	1.949×10^{-21}	1.949×10^{-21}	2.217×10^{-4}	-2.217×10^{-4}	1.950×10^{-21}	7.028×10^{-4}	-7.023×10^{-4}
^{218}Po	6.115	1.403×10^{-24}	1.404×10^{-24}	2.874×10^{-4}	-2.873×10^{-4}	1.405×10^{-24}	9.091×10^{-4}	-9.082×10^{-4}
^{194}Rn	7.862	2.725×10^{-19}	2.726×10^{-19}	1.457×10^{-4}	-1.457×10^{-4}	2.726×10^{-19}	4.613×10^{-4}	-4.611×10^{-4}
^{196}Rn	7.617	5.195×10^{-20}	5.196×10^{-20}	1.578×10^{-4}	-1.578×10^{-4}	5.198×10^{-20}	4.994×10^{-4}	-4.991×10^{-4}

Table 1 (continued)

Nucleus ^{A}Z	Q_p (MeV)	P	$I = 10^{23}$ W/cm^2			$I = 10^{24}$ W/cm^2		
			P^{23}	δP^{23}	δT^{23}	P^{24}	δP^{24}	δT^{24}
^{198}Rn	7.349	7.196×10^{-21}	7.197×10^{-21}	1.722×10^{-4}	-1.721×10^{-4}	7.200×10^{-21}	5.443×10^{-4}	-5.440×10^{-4}
^{200}Rn	7.043	4.433×10^{-22}	4.434×10^{-22}	1.874×10^{-4}	-1.873×10^{-4}	4.436×10^{-22}	5.921×10^{-4}	-5.918×10^{-4}
^{202}Rn	6.774	4.638×10^{-23}	4.639×10^{-23}	2.056×10^{-4}	-2.056×10^{-4}	4.641×10^{-23}	6.494×10^{-4}	-6.489×10^{-4}
^{204}Rn	6.547	6.223×10^{-24}	6.224×10^{-24}	2.231×10^{-4}	-2.231×10^{-4}	6.227×10^{-24}	7.056×10^{-4}	-7.051×10^{-4}
^{206}Rn	6.384	1.425×10^{-24}	1.425×10^{-24}	2.386×10^{-4}	-2.385×10^{-4}	1.426×10^{-24}	7.548×10^{-4}	-7.543×10^{-4}
^{208}Rn	6.261	4.470×10^{-25}	4.471×10^{-25}	2.521×10^{-4}	-2.521×10^{-4}	4.474×10^{-25}	7.974×10^{-4}	-7.967×10^{-4}
^{210}Rn	6.159	1.691×10^{-25}	1.691×10^{-25}	2.644×10^{-4}	-2.643×10^{-4}	1.692×10^{-25}	8.363×10^{-4}	-8.356×10^{-4}
^{212}Rn	6.385	1.812×10^{-24}	1.812×10^{-24}	2.515×10^{-4}	-2.514×10^{-4}	1.813×10^{-24}	7.943×10^{-4}	-7.937×10^{-4}
^{214}Rn	9.208	1.609×10^{-15}	1.609×10^{-15}	1.245×10^{-4}	-1.245×10^{-4}	1.610×10^{-15}	3.948×10^{-4}	-3.947×10^{-4}
^{216}Rn	8.198	4.316×10^{-18}	4.316×10^{-18}	1.597×10^{-4}	-1.596×10^{-4}	4.318×10^{-18}	5.029×10^{-4}	-5.026×10^{-4}
^{218}Rn	7.263	5.514×10^{-21}	5.516×10^{-21}	2.046×10^{-4}	-2.046×10^{-4}	5.518×10^{-21}	6.464×10^{-4}	-6.460×10^{-4}
^{220}Rn	6.405	3.190×10^{-24}	3.191×10^{-24}	2.658×10^{-4}	-2.657×10^{-4}	3.193×10^{-24}	8.409×10^{-4}	-8.402×10^{-4}
^{222}Rn	5.59	5.796×10^{-28}	5.798×10^{-28}	3.558×10^{-4}	-3.557×10^{-4}	5.803×10^{-28}	1.125×10^{-3}	-1.124×10^{-3}
^{202}Ra	7.88	7.889×10^{-20}	7.890×10^{-20}	1.562×10^{-4}	-1.562×10^{-4}	7.893×10^{-20}	4.936×10^{-4}	-4.934×10^{-4}
^{204}Ra	7.637	1.297×10^{-20}	1.297×10^{-20}	1.679×10^{-4}	-1.678×10^{-4}	1.297×10^{-20}	5.312×10^{-4}	-5.309×10^{-4}
^{206}Ra	7.415	1.881×10^{-21}	1.881×10^{-21}	1.790×10^{-4}	-1.789×10^{-4}	1.882×10^{-21}	5.657×10^{-4}	-5.654×10^{-4}
^{208}Ra	7.273	6.633×10^{-22}	6.634×10^{-22}	1.888×10^{-4}	-1.888×10^{-4}	6.637×10^{-22}	5.976×10^{-4}	-5.972×10^{-4}
^{210}Ra	7.151	2.501×10^{-22}	2.502×10^{-22}	1.984×10^{-4}	-1.984×10^{-4}	2.503×10^{-22}	6.272×10^{-4}	-6.268×10^{-4}
^{214}Ra	7.273	7.154×10^{-22}	7.156×10^{-22}	1.973×10^{-4}	-1.972×10^{-4}	7.159×10^{-22}	6.249×10^{-4}	-6.245×10^{-4}
^{216}Ra	9.526	1.982×10^{-15}	1.983×10^{-15}	1.195×10^{-4}	-1.195×10^{-4}	1.983×10^{-15}	3.766×10^{-4}	-3.764×10^{-4}
^{218}Ra	8.54	7.503×10^{-18}	7.505×10^{-18}	1.492×10^{-4}	-1.492×10^{-4}	7.507×10^{-18}	4.717×10^{-4}	-4.714×10^{-4}
^{220}Ra	7.594	1.186×10^{-20}	1.186×10^{-20}	1.900×10^{-4}	-1.899×10^{-4}	1.187×10^{-20}	6.012×10^{-4}	-6.009×10^{-4}
^{222}Ra	6.678	7.823×10^{-24}	7.825×10^{-24}	2.516×10^{-4}	-2.515×10^{-4}	7.829×10^{-24}	7.962×10^{-4}	-7.956×10^{-4}
^{224}Ra	5.789	1.089×10^{-27}	1.090×10^{-27}	3.431×10^{-4}	-3.430×10^{-4}	1.090×10^{-27}	1.086×10^{-3}	-1.085×10^{-3}
^{226}Ra	4.871	5.845×10^{-33}	5.847×10^{-33}	4.937×10^{-4}	-4.934×10^{-4}	5.854×10^{-33}	1.561×10^{-3}	-1.559×10^{-3}
^{208}Th	8.2	1.434×10^{-19}	1.434×10^{-19}	1.513×10^{-4}	-1.513×10^{-4}	1.435×10^{-19}	4.774×10^{-4}	-4.771×10^{-4}
^{210}Th	8.069	4.880×10^{-20}	4.881×10^{-20}	1.574×10^{-4}	-1.574×10^{-4}	4.883×10^{-20}	4.969×10^{-4}	-4.966×10^{-4}
^{212}Th	7.958	2.429×10^{-20}	2.429×10^{-20}	1.644×10^{-4}	-1.644×10^{-4}	2.430×10^{-20}	5.191×10^{-4}	-5.188×10^{-4}
^{214}Th	7.827	8.913×10^{-21}	8.915×10^{-21}	1.714×10^{-4}	-1.714×10^{-4}	8.918×10^{-21}	5.419×10^{-4}	-5.416×10^{-4}
^{216}Th	8.072	5.455×10^{-20}	5.456×10^{-20}	1.636×10^{-4}	-1.636×10^{-4}	5.458×10^{-20}	5.184×10^{-4}	-5.182×10^{-4}
^{218}Th	9.849	2.468×10^{-15}	2.468×10^{-15}	1.130×10^{-4}	-1.130×10^{-4}	2.469×10^{-15}	3.583×10^{-4}	-3.582×10^{-4}
^{220}Th	8.973	2.164×10^{-17}	2.164×10^{-17}	1.383×10^{-4}	-1.383×10^{-4}	2.165×10^{-17}	4.349×10^{-4}	-4.347×10^{-4}
^{222}Th	8.133	1.374×10^{-19}	1.375×10^{-19}	1.712×10^{-4}	-1.712×10^{-4}	1.375×10^{-19}	5.406×10^{-4}	-5.403×10^{-4}
^{224}Th	7.299	4.352×10^{-22}	4.353×10^{-22}	2.189×10^{-4}	-2.188×10^{-4}	4.355×10^{-22}	6.924×10^{-4}	-6.919×10^{-4}
^{226}Th	6.453	2.227×10^{-25}	2.228×10^{-25}	2.836×10^{-4}	-2.835×10^{-4}	2.229×10^{-25}	8.964×10^{-4}	-8.956×10^{-4}
^{228}Th	5.52	7.030×10^{-30}	7.033×10^{-30}	3.941×10^{-4}	-3.939×10^{-4}	7.039×10^{-30}	1.245×10^{-3}	-1.244×10^{-3}
^{230}Th	4.77	2.344×10^{-34}	2.345×10^{-34}	5.420×10^{-4}	-5.417×10^{-4}	2.348×10^{-34}	1.715×10^{-3}	-1.712×10^{-3}
^{232}Th	4.082	1.077×10^{-39}	1.078×10^{-39}	7.586×10^{-4}	-7.580×10^{-4}	1.080×10^{-39}	2.400×10^{-3}	-2.395×10^{-3}
^{216}U	8.531	2.339×10^{-19}	2.339×10^{-19}	1.471×10^{-4}	-1.471×10^{-4}	2.340×10^{-19}	4.661×10^{-4}	-4.659×10^{-4}
^{218}U	8.775	1.172×10^{-18}	1.173×10^{-18}	1.416×10^{-4}	-1.416×10^{-4}	1.173×10^{-18}	4.478×10^{-4}	-4.476×10^{-4}
^{222}U	9.48	8.699×10^{-17}	8.701×10^{-17}	1.261×10^{-4}	-1.261×10^{-4}	8.703×10^{-17}	3.975×10^{-4}	-3.973×10^{-4}
^{224}U	8.628	7.834×10^{-19}	7.835×10^{-19}	1.554×10^{-4}	-1.554×10^{-4}	7.837×10^{-19}	4.904×10^{-4}	-4.902×10^{-4}
^{226}U	7.701	1.503×10^{-21}	1.504×10^{-21}	1.984×10^{-4}	-1.984×10^{-4}	1.504×10^{-21}	6.275×10^{-4}	-6.271×10^{-4}
^{228}U	6.8	1.034×10^{-24}	1.035×10^{-24}	2.602×10^{-4}	-2.601×10^{-4}	1.035×10^{-24}	8.230×10^{-4}	-8.223×10^{-4}
^{230}U	5.993	2.734×10^{-28}	2.735×10^{-28}	3.402×10^{-4}	-3.400×10^{-4}	2.737×10^{-28}	1.076×10^{-3}	-1.074×10^{-3}
^{232}U	5.414	3.194×10^{-31}	3.195×10^{-31}	4.272×10^{-4}	-4.271×10^{-4}	3.198×10^{-31}	1.352×10^{-3}	-1.350×10^{-3}

Table 1 (continued)

Nucleus ^{A}Z	Q_p (MeV)	P	$I = 10^{23}$ W/cm^2			$I = 10^{24}$ W/cm^2		
			P^{23}	δP^{23}	δT^{23}	P^{24}	δP^{24}	δT^{24}
^{234}U	4.858	1.720×10^{-34}	1.721×10^{-34}	5.468×10^{-4}	-5.465×10^{-4}	1.723×10^{-34}	1.730×10^{-3}	-1.727×10^{-3}
^{236}U	4.573	1.303×10^{-36}	1.304×10^{-36}	6.242×10^{-4}	-6.238×10^{-4}	1.306×10^{-36}	1.975×10^{-3}	-1.971×10^{-3}
^{238}U	4.27	5.116×10^{-39}	5.120×10^{-39}	7.279×10^{-4}	-7.274×10^{-4}	5.128×10^{-39}	2.303×10^{-3}	-2.298×10^{-3}
^{228}Pu	7.94	1.801×10^{-21}	1.801×10^{-21}	1.902×10^{-4}	-1.902×10^{-4}	1.802×10^{-21}	6.016×10^{-4}	-6.012×10^{-4}
^{230}Pu	7.178	4.867×10^{-24}	4.868×10^{-24}	2.373×10^{-4}	-2.373×10^{-4}	4.870×10^{-24}	7.500×10^{-4}	-7.494×10^{-4}
^{234}Pu	6.31	3.522×10^{-27}	3.523×10^{-27}	3.253×10^{-4}	-3.252×10^{-4}	3.526×10^{-27}	1.029×10^{-3}	-1.028×10^{-3}
^{236}Pu	5.867	2.204×10^{-29}	2.204×10^{-29}	3.801×10^{-4}	-3.800×10^{-4}	2.206×10^{-29}	1.202×10^{-3}	-1.201×10^{-3}
^{238}Pu	5.593	6.300×10^{-31}	6.303×10^{-31}	4.219×10^{-4}	-4.217×10^{-4}	6.308×10^{-31}	1.334×10^{-3}	-1.332×10^{-3}
^{240}Pu	5.256	6.861×10^{-33}	6.865×10^{-33}	4.844×10^{-4}	-4.841×10^{-4}	6.872×10^{-33}	1.533×10^{-3}	-1.531×10^{-3}
^{242}Pu	4.984	1.096×10^{-34}	1.096×10^{-34}	5.448×10^{-4}	-5.445×10^{-4}	1.098×10^{-34}	1.724×10^{-3}	-1.721×10^{-3}
^{244}Pu	4.666	5.324×10^{-37}	5.328×10^{-37}	6.298×10^{-4}	-6.294×10^{-4}	5.335×10^{-37}	1.993×10^{-3}	-1.989×10^{-3}
^{234}Cm	7.365	1.136×10^{-23}	1.136×10^{-23}	2.394×10^{-4}	-2.393×10^{-4}	1.137×10^{-23}	7.574×10^{-4}	-7.568×10^{-4}
^{236}Cm	7.067	8.844×10^{-25}	8.846×10^{-25}	2.631×10^{-4}	-2.631×10^{-4}	8.851×10^{-25}	8.327×10^{-4}	-8.320×10^{-4}
^{238}Cm	6.67	2.144×10^{-26}	2.145×10^{-26}	2.990×10^{-4}	-2.989×10^{-4}	2.146×10^{-26}	9.458×10^{-4}	-9.449×10^{-4}
^{240}Cm	6.398	1.093×10^{-27}	1.093×10^{-27}	3.272×10^{-4}	-3.271×10^{-4}	1.094×10^{-27}	1.035×10^{-3}	-1.034×10^{-3}
^{242}Cm	6.216	1.350×10^{-28}	1.351×10^{-28}	3.494×10^{-4}	-3.493×10^{-4}	1.352×10^{-28}	1.106×10^{-3}	-1.105×10^{-3}
^{244}Cm	5.902	3.289×10^{-30}	3.290×10^{-30}	3.914×10^{-4}	-3.913×10^{-4}	3.293×10^{-30}	1.239×10^{-3}	-1.237×10^{-3}
^{246}Cm	5.475	1.170×10^{-32}	1.170×10^{-32}	4.593×10^{-4}	-4.591×10^{-4}	1.172×10^{-32}	1.454×10^{-3}	-1.451×10^{-3}
^{248}Cm	5.162	1.189×10^{-34}	1.190×10^{-34}	5.228×10^{-4}	-5.226×10^{-4}	1.191×10^{-34}	1.655×10^{-3}	-1.652×10^{-3}
^{238}Cf	8.13	8.684×10^{-22}	8.685×10^{-22}	2.019×10^{-4}	-2.019×10^{-4}	8.689×10^{-22}	6.384×10^{-4}	-6.380×10^{-4}
^{240}Cf	7.711	3.627×10^{-23}	3.628×10^{-23}	2.268×10^{-4}	-2.267×10^{-4}	3.629×10^{-23}	7.176×10^{-4}	-7.170×10^{-4}
^{242}Cf	7.517	6.678×10^{-24}	6.680×10^{-24}	2.406×10^{-4}	-2.405×10^{-4}	6.683×10^{-24}	7.604×10^{-4}	-7.598×10^{-4}
^{244}Cf	7.329	1.365×10^{-24}	1.365×10^{-24}	2.556×10^{-4}	-2.556×10^{-4}	1.366×10^{-24}	8.088×10^{-4}	-8.082×10^{-4}
^{246}Cf	6.862	1.739×10^{-26}	1.740×10^{-26}	2.941×10^{-4}	-2.940×10^{-4}	1.741×10^{-26}	9.310×10^{-4}	-9.301×10^{-4}
^{248}Cf	6.361	8.377×10^{-29}	8.380×10^{-29}	3.449×10^{-4}	-3.448×10^{-4}	8.386×10^{-29}	1.091×10^{-3}	-1.090×10^{-3}
^{250}Cf	6.129	5.615×10^{-30}	5.617×10^{-30}	3.746×10^{-4}	-3.745×10^{-4}	5.622×10^{-30}	1.186×10^{-3}	-1.185×10^{-3}
^{252}Cf	6.217	1.601×10^{-29}	1.602×10^{-29}	3.682×10^{-4}	-3.681×10^{-4}	1.603×10^{-29}	1.165×10^{-3}	-1.164×10^{-3}
^{254}Cf	5.927	4.888×10^{-31}	4.890×10^{-31}	4.096×10^{-4}	-4.095×10^{-4}	4.894×10^{-31}	1.297×10^{-3}	-1.295×10^{-3}
^{246}Fm	8.379	9.890×10^{-22}	9.892×10^{-22}	1.984×10^{-4}	-1.984×10^{-4}	9.897×10^{-22}	6.268×10^{-4}	-6.264×10^{-4}
^{248}Fm	7.995	5.730×10^{-23}	5.731×10^{-23}	2.195×10^{-4}	-2.194×10^{-4}	5.734×10^{-23}	6.953×10^{-4}	-6.948×10^{-4}
^{250}Fm	7.557	1.480×10^{-24}	1.480×10^{-24}	2.480×10^{-4}	-2.479×10^{-4}	1.481×10^{-24}	7.838×10^{-4}	-7.832×10^{-4}
^{252}Fm	7.154	3.803×10^{-26}	3.804×10^{-26}	2.788×10^{-4}	-2.787×10^{-4}	3.807×10^{-26}	8.819×10^{-4}	-8.812×10^{-4}
^{254}Fm	7.307	1.634×10^{-25}	1.634×10^{-25}	2.697×10^{-4}	-2.696×10^{-4}	1.635×10^{-25}	8.545×10^{-4}	-8.537×10^{-4}
^{256}Fm	7.025	1.154×10^{-26}	1.154×10^{-26}	2.950×10^{-4}	-2.950×10^{-4}	1.155×10^{-26}	9.336×10^{-4}	-9.327×10^{-4}
^{252}No	8.549	7.214×10^{-22}	7.216×10^{-22}	1.976×10^{-4}	-1.976×10^{-4}	7.219×10^{-22}	6.243×10^{-4}	-6.239×10^{-4}
^{254}No	8.226	6.424×10^{-23}	6.425×10^{-23}	2.150×10^{-4}	-2.150×10^{-4}	6.428×10^{-23}	6.791×10^{-4}	-6.786×10^{-4}
^{256}No	8.582	9.518×10^{-22}	9.520×10^{-22}	1.995×10^{-4}	-1.995×10^{-4}	9.524×10^{-22}	6.311×10^{-4}	-6.307×10^{-4}
^{256}Rf	8.926	2.009×10^{-21}	2.010×10^{-21}	1.847×10^{-4}	-1.846×10^{-4}	2.010×10^{-21}	5.851×10^{-4}	-5.848×10^{-4}
^{258}Rf	9.196	1.318×10^{-20}	1.318×10^{-20}	1.759×10^{-4}	-1.759×10^{-4}	1.318×10^{-20}	5.576×10^{-4}	-5.573×10^{-4}
^{260}Sg	9.901	2.377×10^{-19}	2.378×10^{-19}	1.543×10^{-4}	-1.543×10^{-4}	2.378×10^{-19}	4.888×10^{-4}	-4.886×10^{-4}
^{266}Hs	10.346	8.033×10^{-19}	8.034×10^{-19}	1.461×10^{-4}	-1.461×10^{-4}	8.037×10^{-19}	4.623×10^{-4}	-4.621×10^{-4}
^{268}Hs	9.76	2.387×10^{-20}	2.387×10^{-20}	1.649×10^{-4}	-1.648×10^{-4}	2.388×10^{-20}	5.221×10^{-4}	-5.218×10^{-4}
^{270}Hs	9.07	2.579×10^{-22}	2.580×10^{-22}	1.920×10^{-4}	-1.919×10^{-4}	2.581×10^{-22}	6.093×10^{-4}	-6.089×10^{-4}
^{270}Ds	11.117	1.344×10^{-17}	1.344×10^{-17}	1.298×10^{-4}	-1.298×10^{-4}	1.344×10^{-17}	4.102×10^{-4}	-4.100×10^{-4}
^{282}Ds	9.15	7.655×10^{-23}	7.657×10^{-23}	1.992×10^{-4}	-1.992×10^{-4}	7.660×10^{-23}	6.296×10^{-4}	-6.292×10^{-4}
^{286}Cn	9.24	3.165×10^{-23}	3.166×10^{-23}	2.001×10^{-4}	-2.000×10^{-4}	3.167×10^{-23}	6.316×10^{-4}	-6.312×10^{-4}

Table 1 (continued)

Nucleus ^{A}Z	Q_p (MeV)	P	$I = 10^{23}$ W/cm^2			$I = 10^{24}$ W/cm^2		
			P^{23}	δP^{23}	δT^{23}	P^{24}	δP^{24}	δT^{24}
^{286}Fl	10.36	8.791×10^{-21}	8.792×10^{-21}	1.592×10^{-4}	-1.592×10^{-4}	8.795×10^{-21}	5.030×10^{-4}	-5.028×10^{-4}
^{288}Fl	10.076	1.610×10^{-21}	1.610×10^{-21}	1.694×10^{-4}	-1.694×10^{-4}	1.611×10^{-21}	5.365×10^{-4}	-5.362×10^{-4}
^{290}Fl	9.86	4.198×10^{-22}	4.199×10^{-22}	1.789×10^{-4}	-1.788×10^{-4}	4.200×10^{-22}	5.651×10^{-4}	-5.647×10^{-4}
^{290}Lv	11	9.093×10^{-20}	9.094×10^{-20}	1.444×10^{-4}	-1.444×10^{-4}	9.097×10^{-20}	4.565×10^{-4}	-4.563×10^{-4}
^{292}Lv	10.791	2.750×10^{-20}	2.751×10^{-20}	1.507×10^{-4}	-1.507×10^{-4}	2.752×10^{-20}	4.770×10^{-4}	-4.768×10^{-4}
^{294}Og	11.87	2.718×10^{-18}	2.719×10^{-18}	1.271×10^{-4}	-1.271×10^{-4}	2.719×10^{-18}	4.020×10^{-4}	-4.018×10^{-4}

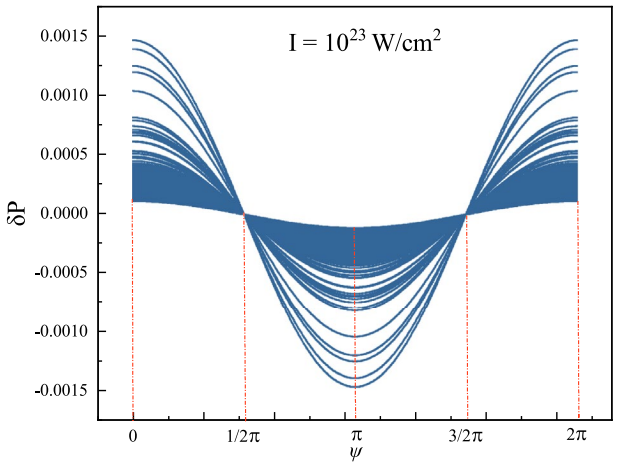

Fig. 2 (Color online) Correlation between δP and ψ for 190 ground-state even–even nuclei

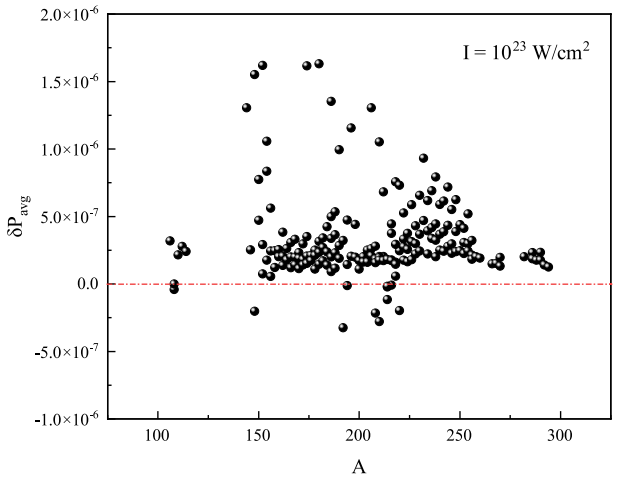

Fig. 3 (Color online) Average effect of a laser on the penetration probability δP_{avg} of the nuclei population with a laser intensity of $I = 10^{23}$ W/cm^2 from a specific direction

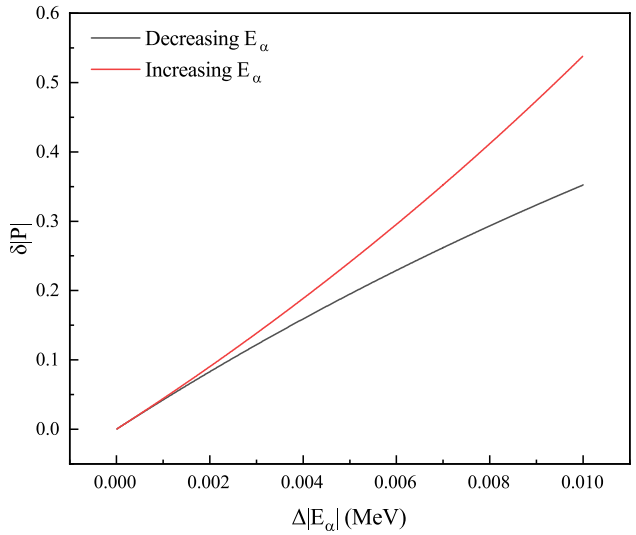

Fig. 4 (Color online) Difference between the absolute value of δP calculated by increasing or decreasing E_α

horizontal axis represents the absolute value of the change in kinetic energy, and the vertical axis represents the absolute value of the change in penetration probability. For any parent nucleus, as E_α increases, the penetration probability increases. Conversely, as E_α decreases, the penetration probability also decreases. In addition, we provide the absolute value of δP corresponding to the case of ^{144}Nd for increasing or decreasing the same value of V in Fig. 5. Different from Fig. 4, the increase in V led to a decrease in the probability of penetration in this figure.

As shown in Figs. 4 and 5, for the parent nucleus ^{144}Nd, the absolute value of P calculated by decreasing the value of V and increasing the value of E_α (which corresponds to the laser direction being the same as the direction of particle emission) is greater than the absolute value of P calculated by increasing the value of V and decreasing the value of E_α (which corresponds to the laser direction being the opposite of the direction of particle emission) for the same transverse coordinates. This means that δP_{avg} obtained by averaging over all α emission

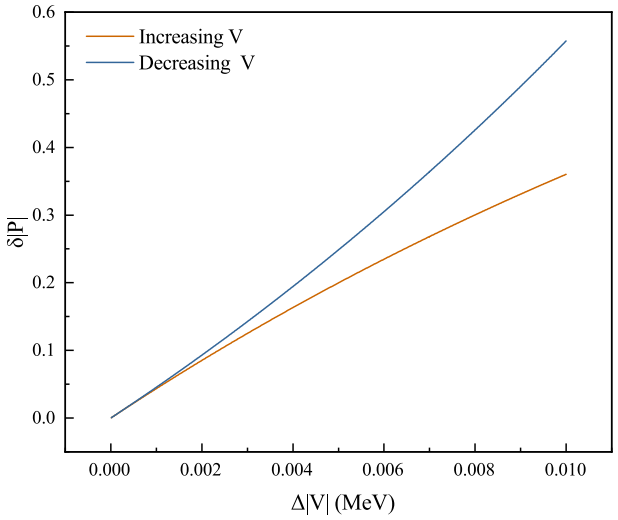

Fig. 5 (Color online) Difference between the absolute value of δP calculated by increasing or decreasing V

directions should be greater than zero for the parent nucleus ^{144}Nd. This conclusion is also supported in Fig. 3, which shows that the suppression and promotion of the α decay penetration probability of the nuclei population by the laser does not cancel completely; a small amount $\delta P_{\rm avg}$ is retained, which is three orders of magnitude lower than δP at $\cos\psi = 0$ under the same laser conditions. This indicates that the relationship between the laser electric field intensity E and δP is not completely linear.

Interestingly, $\delta P_{\rm avg}$ remains positive for most nuclei populations, instead of being equally distributed around zero. To explain this phenomenon, we consider the Taylor expansion in Eq. (2) [71].

$$P(\theta) = \exp[\chi_\theta^{(0)}]\exp[\chi_\theta^{(1)} + \chi_\theta^{(2)} + ...], \tag{22}$$

where $\chi_\theta^{(0)}$, $\chi_\theta^{(1)}$, and $\chi_\theta^{(2)}$ are expressed as

$$\chi_\theta^{(0)} = -\frac{2(2\mu)^{1/2}}{\hbar}\int_{R_{\rm in}(\theta)}^{R_{\rm out}(\theta)}\sqrt{V_{\theta l\rm C}}\,{\rm d}r, \tag{23}$$

$$\chi_\theta^{(1)} = E(t)\times\frac{(2\mu)^{1/2}Z_{\rm eff}\cos\psi}{\hbar}\int_{R_{\rm in}(\theta)}^{R_{\rm out}(\theta)}\frac{r}{\sqrt{V_{\theta l\rm C}}}\,{\rm d}r, \tag{24}$$

$$\chi_\theta^{(2)} = E^2(t)\times\frac{(2\mu)^{1/2}(Z_{\rm eff}\cos\psi)^2}{4\hbar}\int_{R_{\rm in}(\theta)}^{R_{\rm out}(\theta)}\frac{r^2}{V_{\theta l\rm C}^{3/2}}\,{\rm d}r \tag{25}$$

where $V_{\theta l\rm C} = V_l(r) + V_{\rm C}(r,\theta) - E_\alpha$ represents the integrand function without the laser modification. $\chi_\theta^{(0)}$ denotes the penetration probability in a given direction without laser modification. The rate of change of the penetration probability $\delta P(\theta)$ in a given direction can be written as

$$\delta P(\theta) = \chi_\theta^{(1)} + \chi_\theta^{(2)} + ..., \tag{26}$$

Equation (25) indicates that $\chi_\theta^{(2)}$ in Eq. (26) is always positive for any ψ. Assuming $\chi_\theta^{(2)}$ varies in its positivity and negativity with $\cos\psi$ as $\chi_\theta^{(1)}$, then $\delta P_{\rm avg}$ should be distributed around zero on average for all nuclei populations. Because $\chi_\theta^{(2)}$ only has a positive contribution to $\delta P_{\rm avg}$, this leads to a collective upward shift in $\delta P_{\rm avg}$ for all the nuclei populations shown in Fig. 3. This makes the number of nuclei populations with positive $\delta P_{\rm avg}$ higher than those with negative $\delta P_{\rm avg}$. Furthermore, in Fig. 3, the laser direction is arbitrary, which means that the average rate of change of the α decay penetration probability of the nuclei population is not affected by the incident direction of the laser, but only by the laser electric field intensity. Therefore, maintaining the maximum laser intensity yielded a more significant $\delta P_{\rm avg}$. Considering the effect of the spatial shape of the laser, we suggest the use of a circularly polarized laser to obtain a more significant $\delta P_{\rm avg}$ for the nuclei population in future experiments.

4 Summary

In this study, the effect of an extreme laser field on the α decay of ground-state even–even nuclei within a deformed Gamow-like model, which had only one adjustable parameter, was investigated. Results revealed that state-of-the-art lasers have a minor impact on the α decay penetration probability. Moreover, the relationship between ψ and the rate of change of the α decay penetration probability for different nuclei was studied. Furthermore, the average effect of extreme laser fields on the α decay penetration probability of many nuclei with arbitrary α particle-emission angles was calculated. From the results, it was inferred that circularly polarized lasers must be used to obtain a more significant average rate of change in the α decay half-life of nuclei populations in future experiments.

Acknowledgements We thank Prof. Xiao-Hua Li and Dr. Hai-Feng Gui for useful discussions.

Author contributions All authors contributed to the study conception and design. Material preparation, data collection and analysis were performed by Qiong Xiao, Jun-Hao Cheng, Yang-Yang Xu and You-Tian Zou. The first draft of the manuscript was written by Qiong Xiao and all authors commented on previous versions of the manuscript. All authors read and approved the final manuscript.

Data availibility The data that support the findings of this study are openly available in Science Data Bank at https://cstr.cn/31253.11.sciencedb.j00186.00358 and .

Declarations

Conflict of interest The authors declare that they have no conflict of interest.

References

1. J.G. Deng, H.F. Zhang, X.D. Sun, New behaviors of α-particle preformation factors near doubly magic ^{100}Sn*. Chin. Phys. C **46**, 061001 (2022). https://doi.org/10.1088/1674-1137/ac5a9f
2. J.G. Deng, H.F. Zhang, Probing the robustness of $N = 126$ shell closure via the α decay systematics. Eur. Phys. J. A **58**, 165 (2022). https://doi.org/10.1140/epja/s10050-022-00813-8
3. D.M. Deng, Z.Z. Ren, Systematics of α-preformation factors in closed-shell regions. Nucl. Sci. Tech. **27**, 150 (2016). https://doi.org/10.1007/s41365-016-0151-1
4. N. Wan, C. Xu, Z.Z. Ren, Exploring the sensitivity of α-decay half-life to neutron skin thickness for nuclei around ^{208} Pb. Nucl. Sci. Tech. **28**, 22 (2016). https://doi.org/10.1007/s41365-016-0174-7
5. G. Gamow, Zur quantentheorie des atomkernes. Z. Phys. **51**, 204 (1928). https://doi.org/10.1007/BF01343196
6. R.W. Gurney, E.U. Condon, Wave mechanics and radioactive disintegration. Nature **122**, 439 (1928). https://doi.org/10.1038/122439a0
7. D.S. Delion, Universal decay rule for reduced widths. Phys. Rev. C **80**, 024310 (2009). https://doi.org/10.1103/PhysRevC.80.024310
8. K.P. Santhosh, S. Sahadevan, B. Priyanka et al., Systematic study of heavy cluster emission from $^{210-226}$Ra isotopes. Nucl. Phys. A **882**, 49 (2012). https://doi.org/10.1016/j.nuclphysa.2012.04.001
9. J.M. Dong, H.F. Zhang, G. Royer, Proton radioactivity within a generalized liquid drop model. Phys. Rev. C **79**, 054330 (2009). https://doi.org/10.1103/PhysRevC.79.054330
10. X.J. Bao, S.Q. Guo, H.F. Zhang et al., Competition between α -decay and spontaneous fission for super heavy nuclei. J. Phys. G Nucl. Part. Phys. **42**, 085101 (2015). https://doi.org/10.1088/0954-3899/42/8/085101
11. A.N. Andreyev, M. Huyse, P. Van Duppen et al., Signatures of the $Z = 82$ shell closure in α-decay process. Phys. Rev. Lett. **110**, 242502 (2013). https://doi.org/10.1103/PhysRevLett.110.242502
12. Y.T. Oganessian, F.S. Abdullin, P.D. Bailey et al., Synthesis of a new element with atomic number Z=117. Phys. Rev. Lett. **104**, 142502 (2010). https://doi.org/10.1103/PhysRevLett.104.142502
13. A. Sobiczewski, K. Pomorski, Description of structure and properties of superheavy nuclei. Prog. Part. Nucl. Phys. **58**, 292 (2007). https://doi.org/10.1016/j.ppnp.2006.05.001
14. A.B. Balantekin, N. Takigawa, Quantum tunneling in nuclear fusion. Rev. Mod. Phys. **70**, 77 (1998). https://doi.org/10.1103/RevModPhys.70.77
15. H.C. Manjunatha, N. Sowmya, P.S. Damodara Gupta et al., Investigation of decay modes of superheavy nuclei. Nucl. Sci. Tech. **32**, 130 (2021). https://doi.org/10.1007/s41365-021-00967-y
16. Y.Q. Xin, N.N. Ma, J.G. Deng et al., Properties of $Z = 114$ superheavy nuclei. Nucl. Sci. Tech. **32**, 55 (2021). https://doi.org/10.1007/s41365-021-00899-7
17. Y.J. Ren, Z.Z. Ren, New Geiger–Nuttall law for α decay of heavy nuclei. Phys. Rev. C **85**, 044608 (2012). https://doi.org/10.1103/PhysRevC.85.044608
18. T.K. Dong, Z.Z. Ren, New calculations of α-decay half-lives by the Viola–Seaborg formula. Eur. Phys. J. A **26**, 69 (2005). https://doi.org/10.1140/epja/i2005-10142-y
19. H.B. Yang, Z.G. Gan, Z.Y. Zhang et al., New isotope ^{207}Th and odd-even staggering in αdecay energies for nuclei with Zf<82 and N>126. Phys. Rev. C **105**, L051302 (2022). https://doi.org/10.1103/PhysRevC.105.L051302
20. H.B. Yang, Z.G. Gan, Z.Y. Zhang et al., α decay of the new isotope ^{204}Ac. Phys. Lett. B **834**, 137484 (2022). https://doi.org/10.1016/j.physletb.2022.137484
21. L.X. Chen, S.Y. Xu, Z.Y. Zhang et al., Reaction ^{55}Mn + ^{159}Tb: preparation for the synthesis of new elements*. Chin. Phys. C **47**, 054001 (2023). https://doi.org/10.1088/1674-1137/acb9e2
22. N. Kinoshita, M. Paul, Y. Kashiv et al., RRETRACTED: a shorter ^{146}Sm half-life measured and implications for ^{146}Sm-^{142}Nd chronology in the solar system. Science **335**, 1614 (2012). https://doi.org/10.1126/science.1215510
23. H.O.U. Fynbo, C.A. Diget, U.C. Bergmann et al., Revised rates for the stellar triple-α process from measurement of ^{12}C nuclear resonances. Nature **433**, 136 (2005). https://doi.org/10.1038/nature03219
24. J.G. Deng, H.F. Zhang, Correlation between α-particle preformation factor and α decay energy. Phys. Lett. B **816**, 136247 (2021). https://doi.org/10.1016/j.physletb.2021.136247
25. Y.Z. Wang, J.Z. Gu, Z.Y. Hou, Preformation factor for α particles in isotopes near $N = Z$. Phys. Rev. C **89**, 047301 (2014). https://doi.org/10.1103/PhysRevC.89.047301
26. H.F. Zhang, W. Zuo, J.Q. Li et al., α decay half-lives of new superheavy nuclei within a generalized liquid drop model. Phys. Rev. C **74**, 017304 (2006). https://doi.org/10.1103/PhysRevC.74.017304
27. M. Gonçalves, S.B. Duarte, Effective liquid drop description for the exotic decay of nuclei. Phys. Rev. C **48**, 2409 (1993). https://doi.org/10.1103/PhysRevC.48.2409
28. J.G. Deng, H.F. Zhang, Systematic study of α decay half-lives within the generalized liquid drop model with various versions of proximity energies*. Chin. Phys. C **45**, 024104 (2021). https://doi.org/10.1088/1674-1137/abcc5a
29. A. Zdeb, M. Warda, K. Pomorski, Half-lives for α and cluster radioactivity within a Gamow-like model. Phys. Rev. C **87**, 024308 (2013). https://doi.org/10.1103/PhysRevC.87.024308
30. A. Zdeb, M. Warda, K. Pomorski, Half-lives for α and cluster radioactivity in a simple model. Phys. Scr. **T154**, 014029 (2013). https://doi.org/10.1088/0031-8949/2013/T154/014029
31. J.H. Cheng, J.L. Chen, J.G. Deng et al., Systematic study of α decay half-lives based on Gamow-like model with a screened electrostatic barrier. Nucl. Phys. A **987**, 350 (2019). https://doi.org/10.1016/j.nuclphysa.2019.05.002
32. B. Buck, A.C. Merchant, S.M. Perez, New look at α decay of heavy nuclei. Phys. Rev. Lett. **65**, 2975 (1990). https://doi.org/10.1103/PhysRevLett.65.2975
33. C. Xu, Z.Z. Ren, Global calculation of α-decay half-lives with a deformed density-dependent cluster model. Phys. Rev. C **74**, 014304 (2006). https://doi.org/10.1103/PhysRevC.74.014304
34. C. Xu, Z.Z. Ren, Favored α-decays of medium mass nuclei in density-dependent cluster model. Nucl. Phys. A **760**, 303 (2005). https://doi.org/10.1016/j.nuclphysa.2005.06.011
35. X.D. Sun, P. Guo, X.H. Li, Systematic study of α decay half-lives for even-even nuclei within a two-potential approach. Phys. Rev. C **93**, 034316 (2016). https://doi.org/10.1103/PhysRevC.93.034316
36. J.G. Deng, J.C. Zhao, D. Xiang et al., Systematic study of unfavored α-decay half-lives of closed-shell nuclei related to ground and isomeric states. Phys. Rev. C **96**, 024318 (2017). https://doi.org/10.1103/PhysRevC.96.024318
37. J.G. Deng, J.C. Zhao, P.C. Chu et al., Systematic study of α decay of nuclei around the $Z = 82, N = 126$ shell closures within the cluster-formation model and proximity potential 1977 formalism. Phys. Rev. C **97**, 044322 (2018). https://doi.org/10.1103/PhysRevC.97.044322

38. C. Xu, Z.Z. Ren, New deformed model of α-decay half-lives with a microscopic potential. Phys. Rev. C **73**, 041301 (2006). https://doi.org/10.1103/PhysRevC.73.041301
39. M. Ismail, W.M. Seif, A. Adel et al., Alpha-decay of deformed superheavy nuclei as a probe of shell closures. Nucl. Phys. A **958**, 202 (2017). https://doi.org/10.1016/j.nuclphysa.2016.11.010
40. Z.Z. Ren, C. Xu, Theoretical calculations on α-decay half-lives by the density-dependent cluster model. Mod. Phys. Lett. A **23**, 2597 (2008). https://doi.org/10.1142/S0217732308029885
41. D.D. Ni, Z.Z. Ren, T.K. Dong et al., Unified formula of half-lives for α decay and cluster radioactivity. Phys. Rev. C **78**, 044310 (2008). https://doi.org/10.1103/PhysRevC.78.044310
42. V.E. Viola, G.T. Seaborg, Nuclear systematics of the heavy elements-II Lifetimes for alpha, beta and spontaneous fission decay. J. Inorg. Nucl. Chem. **28**, 741 (1966). https://doi.org/10.1016/0022-1902(66)80412-8
43. G. Royer, Alpha emission and spontaneous fission through quasi-molecular shapes. J. Phys. G Nucl. Part. Phys. **26**, 1149 (2000). https://doi.org/10.1088/0954-3899/26/8/305
44. C. Qi, F.R. Xu, R.J. Liotta et al., Microscopic mechanism of charged-particle radioactivity and generalization of the Geiger–Nuttall law. Phys. Rev. C **80**, 044326 (2009). https://doi.org/10.1103/PhysRevC.80.044326
45. C. Qi, F.R. Xu, R.J. Liotta et al., Universal Decay law in charged-particle emission and exotic cluster radioactivity. Phys. Rev. Lett. **103**, 072501 (2009). https://doi.org/10.1103/PhysRevLett.103.072501
46. D.N. Poenaru, R.A. Gherghescu, W. Greiner, Single universal curve for cluster radioactivities and α decay. Phys. Rev. C **83**, 014601 (2011). https://doi.org/10.1103/PhysRevC.83.014601
47. D. Strickland, G. Mourou, Compression of amplified chirped optical pulses. Opt. Commun. **56**, 219 (1985). https://doi.org/10.1016/0030-4018(85)90120-8
48. R. Betti, O.A. Hurricane, Inertial-confinement fusion with lasers. Nat. Phys. **12**, 435 (2016). https://doi.org/10.1038/nphys3736
49. M.J.C. van Gemert, A.J. Welch, Time constants in thermal laser medicine. Laser. Surg. Med. **9**, 405 (1989). https://doi.org/10.1002/lsm.1900090414
50. N.V. Zamfir, Nuclear physics with 10 PW laser beams at extreme light infrastructure-nuclear physics (ELI-NP). Eur. Phys. J. Spec. Top. **223**, 1221 (2014). https://doi.org/10.1140/epjst/e2014-02176-0
51. B.S. Xie, Z.L. Li, S. Tang, Electron-positron pair production in ultrastrong laser fields. Matter Radiat. Extrem. **2**, 225 (2017). https://doi.org/10.1016/j.mre.2017.07.002
52. S.N. Chen, F. Negoita, K. Spohr et al., Extreme brightness laser-based neutron pulses as a pathway for investigating nucleosynthesis in the laboratory. Matter Radiat. Extrem. **4**, 054402 (2019). https://doi.org/10.1063/1.5081666
53. S.M. Weng, Z.M. Sheng, M. Murakami et al., Optimization of hole-boring radiation pressure acceleration of ion beams for fusion ignition. Matter Radiat. Extrem. **3**, 28 (2018). https://doi.org/10.1016/j.mre.2017.09.002
54. J.W. Yoon, Y.G. Kim, I.W. Choi et al., Realization of laser intensity over 10^{23}W/cm^2. Optica **8**, 630 (2021). https://doi.org/10.1364/OPTICA.420520
55. Ş Mişicu, M. Rizea, Laser-assisted proton radioactivity of spherical and deformed nuclei. J. Phys. G Nucl. Part. Phys. **46**, 115106 (2019). https://doi.org/10.1088/1361-6471/ab1d7c
56. K.A. Tanaka, K.M. Spohr, D.L. Balabanski et al., Current status and highlights of the ELI-NP research program. Matter Radiat. Extrem. **5**, 024402 (2020). https://doi.org/10.1063/1.5093535
57. G.M. Maria, Über Elementarakte mit zwei Quantensprüngen. Ann. Phys. Lpz. **401**, 273 (1931). https://doi.org/10.1002/andp.19314010303
58. J.T. Qi, L.B. Fu, X. Wang, Nuclear fission in intense laser fields. Phys. Rev. C **102**, 064629 (2020). https://doi.org/10.1103/PhysRevC.102.064629
59. W. Wang, J. Zhou, B.Q. Liu et al., Exciting the isomeric ^{229}Th nuclear state via laser-driven electron recollision. Phys. Rev. Lett. **127**, 052501 (2021). https://doi.org/10.1103/PhysRevLett.127.052501
60. W.J. Lv, H. Duan, J. Liu, Enhanced deuterium-tritium fusion cross sections in the presence of strong electromagnetic fields. Phys. Rev. C **100**, 064610 (2019). https://doi.org/10.1103/PhysRevC.100.064610
61. S.A. Ghinescu, D.S. Delion, Coupled-channels analysis of the α decay in strong electromagnetic fields. Phys. Rev. C **101**, 044304 (2020). https://doi.org/10.1103/PhysRevC.101.044304
62. S.W. Liu, H. Duan, D.F. Ye et al., Deuterium-tritium fusion process in strong laser fields: semiclassical simulation. Phys. Rev. C **104**, 044614 (2021). https://doi.org/10.1103/PhysRevC.104.044614
63. J. Feng, W.Z. Wang, C.B. Fu et al., Femtosecond pumping of nuclear isomeric states by the Coulomb collision of ions with quivering electrons. Phys. Rev. Lett. **128**, 052501 (2022). https://doi.org/10.1103/PhysRevLett.128.052501
64. Ş Mişicu, the refractive scattering of loosely bound nuclei in arbitrarily polarized laser fields. Phys. Rev. C **106**, 034612 (2022). https://doi.org/10.1103/PhysRevC.106.034612
65. H.M.C. Cortés, C. Müller, C.H. Keitel et al., Nuclear recollisions in laser-assisted α decay. Phys. Lett. B **723**, 401 (2013). https://doi.org/10.1016/j.physletb.2013.05.025
66. Ş Mişicu, M. Rizea, α-Decay in ultra-intense laser fields. J. Phys. G Nucl. Part. Phys. **40**, 095101 (2013). https://doi.org/10.1088/0954-3899/40/9/095101
67. Ş Mişicu, M. Rizea, Speeding of α decay in strong laser fields. Open Phys. **14**, 81 (2016). https://doi.org/10.1515/phys-2016-0001
68. J.T. Qi, T. Li, R.H. Xu et al., α decay in intense laser fields: calculations using realistic nuclear potentials. Phys. Rev. C **99**, 044610 (2019). https://doi.org/10.1103/PhysRevC.99.044610
69. D.P. Kis, R. Szilvasi, Three dimensional α-tunneling in intense laser fields. J. Phys. G Nucl. Part. Phys. **45**, 045103 (2018). https://doi.org/10.1088/1361-6471/aab0d5
70. D. Bai, Z.Z. Ren, α Decays in superstrong static electric fields*. Commun. Theor. Phys. **70**, 559 (2018). https://doi.org/10.1088/0253-6102/70/5/559
71. J.H. Cheng, W.Y. Zhang, Q. Xiao et al., Laser-assisted deformed α decay of the ground state even-even nuclei (2023). arXiv preprint arXiv:2307.02095. https://doi.org/10.48550/arXiv.2307.02095
72. J.H. Cheng, Y. Li, T.P. Yu, Systematic study of laser-assisted proton radioactivity from deformed nuclei. Phys. Rev. C **105**, 024312 (2022). https://doi.org/10.1103/PhysRevC.105.024312
73. F. Queisser, R. Schützhold, Dynamically assisted nuclear fusion. Phys. Rev. C **100**, 041601 (2019). https://doi.org/10.1103/PhysRevC.100.041601
74. Ş Mişicu, F. Carstoiu, Fraunhofer and refractive scattering of heavy ions in strong laser fields. Eur. Phys. J. A **54**, 90 (2018). https://doi.org/10.1140/epja/i2018-12525-3
75. Q. Xiao, J.H. Cheng, B.L. Wang et al., Half-lives for proton emission and α decay within the deformed Gamow-like model. J. Phys. G Nucl. Part. Phys. **50**, 085102 (2023). https://doi.org/10.1088/1361-6471/acdfeb
76. N. Takigawa, T. Rumin, N. Ihara, Coulomb interaction between spherical and deformed nuclei. Phys. Rev. C **61**, 044607 (2000). https://doi.org/10.1103/PhysRevC.61.044607
77. M. Ismail, W.M. Seif, H. El-Gebaly, On the Coulomb interaction between spherical and deformed nuclei. Phys. Lett. B **563**, 53 (2003). https://doi.org/10.1016/S0370-2693(03)00600-2

78. G.L. Zhang, X.Y. Le, Z.H. Liu, Coulomb potentials between spherical and deformed nuclei. Chin. Phys. Lett. **25**, 1247 (2008). https://doi.org/10.1088/0256-307x/25/4/023
79. J.M. Dong, W. Zuo, J.Z. Gu et al., α-decay half-lives and Q_α values of superheavy nuclei. Phys. Rev. C **81**, 064309 (2010). https://doi.org/10.1103/PhysRevC.81.064309
80. C. Xu, Z.Z. Ren, α decay of nuclei in extreme cases. Phys. Rev. C **69**, 024614 (2004). https://doi.org/10.1103/PhysRevC.69.024614
81. J.W. Yoon, C. Jeon, J. Shin et al., Achieving the laser intensity of $5.5\times10^{23}\mathrm{W}/cm^2$ with a wavefront-corrected multi-PW laser. Opt. Express **27**, 20412 (2019). https://doi.org/10.1364/OE.27.020412
82. W.J. Huang, M. Wang, F.G. Kondev et al., The AME 2020 atomic mass evaluation (I). Evaluation of the input data and adjustment procedures. Chin. Phys. C **45**, 030002 (2021). https://doi.org/10.1088/1674-1137/abddb0
83. M. Wang, W.J. Huang, F.G. Kondev et al., The AME 2020 atomic mass evaluation (II). Tables, graphs, and References. Chin. Phys. C **45**, 030003 (2021). https://doi.org/10.1088/1674-1137/abddaf
84. P. Möller, A.J. Sierk, T. Ichikawa et al., Nuclear ground-state masses and deformations: FRDM(2012). Atom. Data Nucl. Data **109**, 1 (2016). https://doi.org/10.1016/j.adt.2015.10.002